INTERNATIONAL STANDARD

ISO 15367-2

First edition
2005-03-15

Lasers and laser-related equipment — Test methods for determination of the shape of a laser beam wavefront —

Part 2: Shack-Hartmann sensors

Lasers et équipements associés aux lasers — Méthodes d'essai pour la détermination de la forme du front d'onde du faisceau laser —

Partie 2: Senseurs Shack-Hartmann

Reference number
ISO 15367-2:2005(E)

ISO copyright office
Case postale 56 • CH-1211 Geneva 20
Tel. + 41 22 749 01 11
Fax + 41 22 749 09 47
E-mail copyright@iso.org
Web www.iso.org

Published in Switzerland

Contents

Page

Foreword

ISO (the International Organization for Standardization) is a worldwide federation of national standards bodies (ISO member bodies). The work of preparing International Standards is normally carried out through ISO technical committees. Each member body interested in a subject for which a technical committee has been established has the right to be represented on that committee. International organizations, governmental and non-governmental, in liaison with ISO, also take part in the work. ISO collaborates closely with the International Electrotechnical Commission (IEC) on all matters of electrotechnical standardization.

International Standards are drafted in accordance with the rules given in the ISO/IEC Directives, Part 2.

The main task of technical committees is to prepare International Standards. Draft International Standards adopted by the technical committees are circulated to the member bodies for voting. Publication as an International Standard requires approval by at least 75 % of the member bodies casting a vote.

Attention is drawn to the possibility that some of the elements of this document may be the subject of patent rights. ISO shall not be held responsible for identifying any or all such patent rights.

ISO 15367-2 was prepared by Technical Committee ISO/TC 172, *Optics and photonics*, Subcommittee SC 9, *Electro-optical systems*.

ISO 15367 consists of the following parts, under the general title *Lasers and laser-related equipment — Test methods for determination of the shape of a laser beam wavefront*:

— *Part 1: Terminology and fundamental aspects*

— *Part 2: Shack-Hartmann sensors*

Introduction

Characterization of the beam propagation behaviour is necessary in many areas of both laser system development and industrial laser applications. For example, the design of resonator or beam delivery optics strongly relies on detailed and quantitative information over the directional distribution of the emitted radiation. On-line recording of the laser beam wavefront can also accomplish an optimization of the beam focusability in combination with adaptive optics. Other relevant areas are the monitoring and possible reduction of thermal lensing effects, on-line resonator adjustment, laser safety considerations, or “at wavelength” testing of optics including Zernike analysis.

There are four sets of parameters that are relevant for the laser beam propagation:

— power (energy) density distribution (ISO 13694);

— beam widths, divergence angles and beam propagation ratios (ISO 11146-1 and ISO 11146-2);

— wavefront (phase) distribution (ISO 15367-1 and this part of ISO 15367);

— spatial beam coherence (no current standard available).

In general, a complete characterization requires the knowledge of the mutual coherence function or spectral density function, at least in one transverse plane. Although the determination of those distributions is possible, the experimental effort is large and commercial instruments capable of measuring these quantities are still not available. Hence, the scope of this standard does not extend to such a universal beam description but is limited to the measurement of the wavefront, which is equivalent to the phase distribution in case of spatially coherent beams. As a consequence, an exact prediction of beam propagation is achievable only in the limiting case of high lateral coherence.

A number of phase or wavefront gradient measuring instruments are capable of determining the wavefront or phase distribution. These include, but are not limited to, the lateral shearing interferometer, the Hartmann and Shack-Hartmann wavefront sensor, and the Moiré deflectometer. In these instruments, the gradients of either wavefront or phase are measured, from which the two-dimensional phase distribution can be reconstructed.

In this document, only Hartmann and Shack-Hartmann wavefront sensors are considered in detail, as they are able to measure the wavefront of both fully coherent and partially coherent beams. A considerable number of such instruments are commercially available.

The main advantages of the Hartmann technique are

— wide dynamic range,

— high optical efficiency,

— suitability for partially coherent beams,

— no requirement of spectral purity,

— no ambiguity with respect to 2π increment in phase angle,

— wavefronts can be acquired/analysed in a single measurement.

Instruments which are capable of direct phase or wavefront measurement, as, e.g. self-referencing interferometers, are outside the scope of this part of ISO 15367.

Lasers and laser-related equipment — Test methods for determination of the shape of a laser beam wavefront —

Part 2: Shack-Hartmann sensors

1 Scope

This part of ISO 15367 specifies methods for measurement and evaluation of the wavefront distribution function in a transverse plane of a laser beam utilizing Hartmann or Shack-Hartmann wavefront sensors. This part of ISO 15367 is applicable to fully coherent, partially coherent and general astigmatic laser beams, both for pulsed and continuous operation.

Furthermore, reliable numerical methods for both zonal and modal reconstruction of the two-dimensional wavefront distribution together with their uncertainty are described. The knowledge of the wavefront distribution enables the determination of several wavefront parameters that are defined in ISO 15367-1.

2 Normative references

The following referenced documents are indispensable for the application of this document. For dated references, only the edition cited applies. For undated references, the latest edition of the referenced document (including any amendments) applies.

ISO 11145, *Optics and optical instruments — Lasers and laser-related equipment — Vocabulary and symbols*

ISO 13694, *Optics and optical instruments — Lasers and laser-related equipment — Test methods for laser beam power (energy) density distribution*

ISO 15367-1:2003, *Lasers and laser-related equipment — Test methods for determination of the shape of a laser beam wavefront — Part 1: Terminology and fundamental aspects*

3 Terms and definitions

For the purposes of this document, the terms and definitions given in ISO 11145 and ISO 15367-1 as well as the following apply.

3.1
array element spacing
d_x, d_y
distance between the centres of adjacent pinholes or lenslets in x and y direction

3.2
sub-aperture screen to detector spacing
L_H
spacing of the sub-aperture screen (lenslet array or Hartmann screen) to the detector array

NOTE For Shack-Hartmann sensors this is often set to the lenslet focal length.

3.3
lenslet focal length
f
focal length of the lenslets for a Shack-Hartmann sensor

3.4
sub-aperture width
d_{s}
aperture width of the pinholes of a Hartmann screen or lenslets of a Shack-Hartmann array, respectively

3.5
angular dynamic range
$\beta_{\max}$
maximum usable angular range of Hartmann or Shack-Hartmann sensors

NOTE For square apertures, the angular dynamic range is given by

$$\beta_{\max} = \frac{d_x}{2L_{\mathrm{H}}} - \frac{\lambda}{d_x}$$

3.6
wavefront measurement repeatability
$w_{\mathrm{r,rms}}$
root-mean-square (r.m.s.) difference between single subsequent measurements $w_n(x, y)$ of the same wavefront and the average wavefront $\bar{w}(x, y)$

$$w_{\mathrm{r,rms}} = \frac{1}{k}\sum_{n=1}^{k}\sqrt{\frac{\sum_x\sum_y E_n(x,y)\left[w_n(x,y)-\bar{w}(x,y)\right]^2}{\sum_x\sum_y E_n(x,y)} - \left(\frac{\sum_x\sum_y E_n(x,y)\left[w_n(x,y)-\bar{w}(x,y)\right]}{\sum_x\sum_y E_n(x,y)}\right)^2}$$

where

n is the number of the measurement;

k is the number of samples taken;

$$\bar{w}(x,y) = \frac{\sum_{n=1}^{k} E_n(x,y)\times w_n(x,y)}{\sum_{n=1}^{k} E_n(x,y)}$$

3.7
wavefront measurement accuracy
$w_{\mathrm{a,rms}}$
average of the r.m.s. difference between a reference wavefront w_{r} and the tilt-corrected wavefront $w_{\mathrm{tc},n}$ after various amounts of tilt θ_n have been applied to the reference wavefront

$$w_{\mathrm{a,rms}} = \frac{1}{k}\sum_{n=1}^{k}\sqrt{\frac{\sum_x\sum_y E_n(x,y)\left[w_{\mathrm{tc},n}(x,y)-w_{\mathrm{r}}(x,y)\right]^2}{\sum_x\sum_y E_n(x,y)}}$$

where

n is the nth measurement of the wavefront with tilt $\theta_{x,n}$ and $\theta_{y,n}$ applied;

k is the number of samples taken;

$w_{\mathrm{tc},n}$ is the tilt-corrected wavefront as follows:

$$w_{\mathrm{tc},n}(x,y) = w_n(x,y) - \theta_{x,n}x - \theta_{y,n}y$$

NOTE See also ISO 15367-1:2003, 3.4.7.

4 Symbols and units

Table 1 — Symbols and units

Symbol	Parameter	Units	Defined in
$E(x, y)$, $H(x, y)$	power (energy) density distribution	W/cm^2, J/cm^2	ISO 13694
x, y, z	mechanical axes (Cartesian coordinates)	mm	ISO 15367-1:2003, 3.1.5
z	beam axis	mm	ISO 15367-1:2003, 3.1.5
λ	wavelength	nm	
z_{m}	location of measurement plane	mm	ISO 15367-1:2003, 3.1.4
$w(x, y)$	average wavefront shape	nm	ISO 15367-1:2003, 3.1.1
$\Phi(x, y)$	phase distribution	rad	ISO 15367-1:2003, 3.1.1, Note 1
$w_{\mathrm{c}}(x, y)$	corrected wavefront	nm	ISO 15367-1:2003, 3.4.2
$s(x, y)$	approximating spherical surface	—	ISO 15367-1:2003, 3.4.3
R_{ss}	defocus or radius of best sphere	mm	ISO 15367-1:2003, 3.4.5
$w_{\mathrm{AF}}(x, y)$	wavefront aberration function	nm	ISO 15367-1:2003, 3.4.6
w_{PV}	wavefront irregularity	nm	
w_{rms}	weighted r.m.s. deformation	nm	ISO 15367-1:2003, 3.4.7
d_x, d_y	array element spacing	mm	3.1
L_{H}	sub-aperture screen to detector spacing	mm	3.2
f	lenslet focal length	mm	3.3
d_{p}	spot size	µm	
d_{s}	sub-aperture width	µm	3.4
β_{max}	angular dynamic range	mrad	3.5
$(x_{\mathrm{c}}, y_{\mathrm{c}})_{ij}$	beam centroid coordinates in sub-aperture ij i.e. the first order moments of the power density distribution in sub-aperture ij	mm	ISO 11146-1
$(x_{\mathrm{r}}, y_{\mathrm{r}})_{ij}$	reference beam coordinates in sub-aperture ij	mm	
$(\beta_x, \beta_y)_{ij}$	local wavefront gradient components (tilt, tip)	—	ISO 15367-1:2003, 3.5.1, 3.5.3
$w_{\mathrm{r,rms}}$	wavefront measurement repeatability	nm	3.6
$w_{\mathrm{a,rms}}$	wavefront measurement accuracy	nm	3.7
$\boldsymbol{B}$	geometry matrix in wavefront reconstruction algorithms	—	
$\boldsymbol{C}$	covariance matrix	—	

5 Test principle of Hartmann and Shack-Hartmann wavefront sensors

The Hartmann principle is based on a subdivision of the beam into a number of beamlets. This is either accomplished by an opaque screen with pinholes placed on a regular grid (Hartmann sensor), or by a lenslet or micro-lens array (Shack-Hartmann sensor), resulting in an average wavefront gradient sampling (see Figure 1) and a better radiation collection efficiency. The power (energy) density distribution behind the array is recorded by a position sensitive detector, most commonly a CCD sensor or an array of quadrant detectors (quadcells). The detector signals can be accumulated by a computerized data acquisition and analysis system.

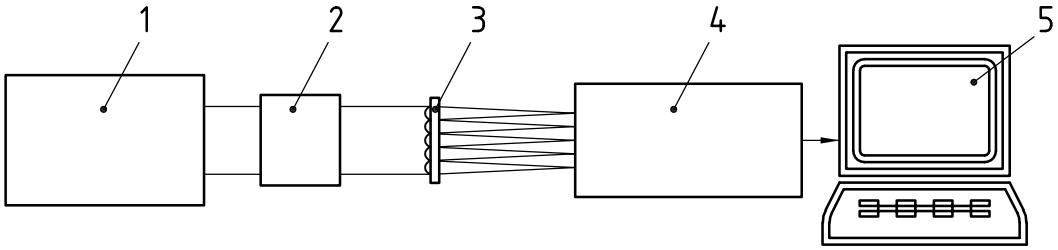

Key

1 laser
2 attenuator
3 lenslet array
4 position sensitive detector
5 data acquisition and analysis system

Figure 1 — Experimental arrangement for wavefront measurement using Shack-Hartmann technique

The position of the beamlet centroids shall be determined within each sub-aperture, both for the beam under test and a reference source, preferably a collimated laser beam. The displacements of the centroids with respect to the reference represent the local wavefront gradients, from which the wavefront $w(x, y)$ is reconstructed by direct integration or modal fitting techniques (see Clause 8).

The type, manufacturer and model identifier of the instrument used for Hartmann or Shack-Hartmann wavefront measurement, as well as the array size and the lens/hole spacing, shall be recorded in the test report.

6 Measurement arrangement and test procedure

6.1 General

Questions concerning different laser types, laser safety, test environment, beam modification (including sampling/attenuation and beam manipulating optics) as well as general requirements on detectors to be employed for phase gradient measurements are treated in ISO 15367-1.

All details on the beam sampling and attenuating optics shall be recorded in the test report.

6.2 Detector system

The detector system used for Hartmann and Shack-Hartmann wavefront measurements shall consist of two elements:

a) a device for segmentation of the beam under test into ray bundles (sub-aperture screen), for example an array of (refractive or diffractive) lenslets (Shack-Hartmann) or a pinhole array (Hartmann).

b) a position sensitive detector (e.g. a CCD camera) positioned at a distance L_H behind the segmenting array (L_H may be set to f in case of Shack-Hartmann detector, or an appropriate correction may be applied).

The detector area shall be partitioned into sub-apertures corresponding to the segmenting array used for subdivision of the beam. Most commonly, an orthogonal array of lenslets/pinholes with a fixed spacing d_x, d_y (in x-, y-direction, respectively) is employed. In this case the detector array shall be partitioned into $N \times M$ rectangular sub-apertures with a spacing d_x, d_y and indexed (ij).

The angular dynamic range of the wavefront sensor with respect to the wavefront variation is directly related to the ratio of the size of the spots generated on the detector to the size of the sub-apertures. To avoid overlapping, the spot size shall be smaller than the sub-aperture size. According to the local wavefront gradient, the spot of a sub-aperture moves towards the border of its assigned region on the detector. If the spot crosses the border, its position may not be correctly obtained anymore. This effect limits the angular dynamic range of the sensor.

For Shack-Hartmann sensors, the spot size d_p is approximately given by

$$d_p = 2\frac{\lambda f}{d_s} \tag{1}$$

where

f is the focal length of the lenslets;

d_s is the width of the square lenslet apertures;

and where it is assumed that the sub-aperture screen to detector spacing equals the focal length. The displacement Δx of a spot due to a horizontal local wavefront gradient β_x at its corresponding sub-aperture is given by

$$\Delta x = \beta_x \times f \tag{2}$$

The maximum allowed displacement Δx_{max} to prevent the spot from crossing its assigned region is

$$\Delta x_{max} = \frac{1}{2}(d_x - d_p) \tag{3}$$

and the according maximum horizontal wavefront gradient

$$\beta_{x,max} = \frac{d_x}{2f} - \frac{\lambda}{d_s} \tag{4}$$

If the size of the lenslet aperture d_s equals the array element spacing d_x, the maximum horizontal wavefront gradient yields

$$\beta_{x,max} = \frac{d_x}{2f} - \frac{\lambda}{d_x} \tag{5}$$

Thus, to avoid spot overlap, the focal length of the lenslets is required to be less than $d_x^2/2\lambda$. To achieve a useful dynamic range and minimize cross talk, the focal length shall be less than $2d_x/5\lambda$. A smaller focal length will result in a greater angular dynamic range, but may also result in greater measurement uncertainty. For the vertical direction a similar expression holds.

In the case of round lenslet apertures of diameter d_s, the maximum wavefront gradient is given by

$$\beta_{x,\max} = \frac{d_x}{2f} - 1{,}22\frac{\lambda}{d_s} \tag{6}$$

If the size of the lenslet aperture d_s equals the array element spacing d_x, the maximum horizontal wavefront gradient yields

$$\beta_{x,\max} = \frac{d_x}{2f} - 1{,}22\frac{\lambda}{d_x} \tag{7}$$

and hence, to achieve a useful dynamic range, the focal length shall be less than $d_x^2 / 2\lambda$.

For Hartmann sensors the spot size d_p is approximately given by

$$d_p = 2\frac{\lambda L_H}{d_s} \tag{8}$$

where

d_s is the width of the square screen apertures;

L_H is the sub-aperture screen to detector spacing.

This approximation is only valid for $L_H \gg d_x^2/\lambda$. The displacement Δx of a spot due to a horizontal local wavefront gradient β_x at its corresponding sub-aperture is given by

$$\Delta x = \beta_x \times L_H \tag{9}$$

The according maximum horizontal wavefront gradient is

$$\beta_{x,\max} = \frac{d_x}{2L_H} - \frac{\lambda}{d_s} \tag{10}$$

Thus, to avoid spot overlap the ratio, L_H / d_s is required to be less than $d_x / 2\lambda$. To achieve a useful dynamic range and minimize cross talk, the ratio L_H / d_s shall be less than $2d_x / 5\lambda$. A smaller ratio will result in a greater angular dynamic range, but may also result in greater measurement uncertainty. For the vertical direction, a similar expression holds.

In the case of round screen apertures of diameter d_s, the maximum wavefront gradient is given by

$$\beta_{x,\max} = \frac{d_x}{2L_H} - 1{,}22\frac{\lambda}{d_s} \tag{11}$$

and hence, to achieve a useful dynamic range, the ratio L_H / d_s shall be less than $d_x / 2\lambda$.

NOTE The dynamic range can be extended from this definition by a number of software algorithms. These algorithms can result from scaling of the sub-aperture grid mapping or other image processing algorithm.

The uncertainty of the measurement is related to the signal-to-noise ratio of the detector and to the number of detector elements covered by the spots. The uncertainty depends upon the characteristics of the detector (detector element size and signal-to-noise ratio) and the geometric screen parameters (distance to the detector, array element spacing, size of sub-apertures and, for Shack-Hartmann sensors, focal length). For accurate measurement, it is necessary that the lenslet/pinhole spots illuminate at least two detector elements in each direction.

Since the uncertainty in the measurements is directly related to the signal-to-noise ratio, the dynamic range of the detector with respect to power (energy) density shall be at least 100:1.

For a proper evaluation of the spot positions, the spatial resolution of the detector shall be at least two times greater than the spacing of the lenslet or pinhole array d_x, d_y.

6.3 Measurement

6.3.1 Alignment

The laser beam to be analysed and the optics employed for beam manipulation shall be adjusted coaxial to the phase measuring instrument, which is positioned in the measurement plane z_m.

6.3.2 Setting of sub-apertures

While monitoring the spot distribution produced by the lenslet or pinhole array with the help of the two-dimensional detector array, the spots shall be properly centered with respect to the detector grid. In particular, each detector sub-area shall contain only one single spot (see Figure 2). Centering of the spot distribution is achieved either by lateral movement of the detector grid, or by tilting the entire detector system.

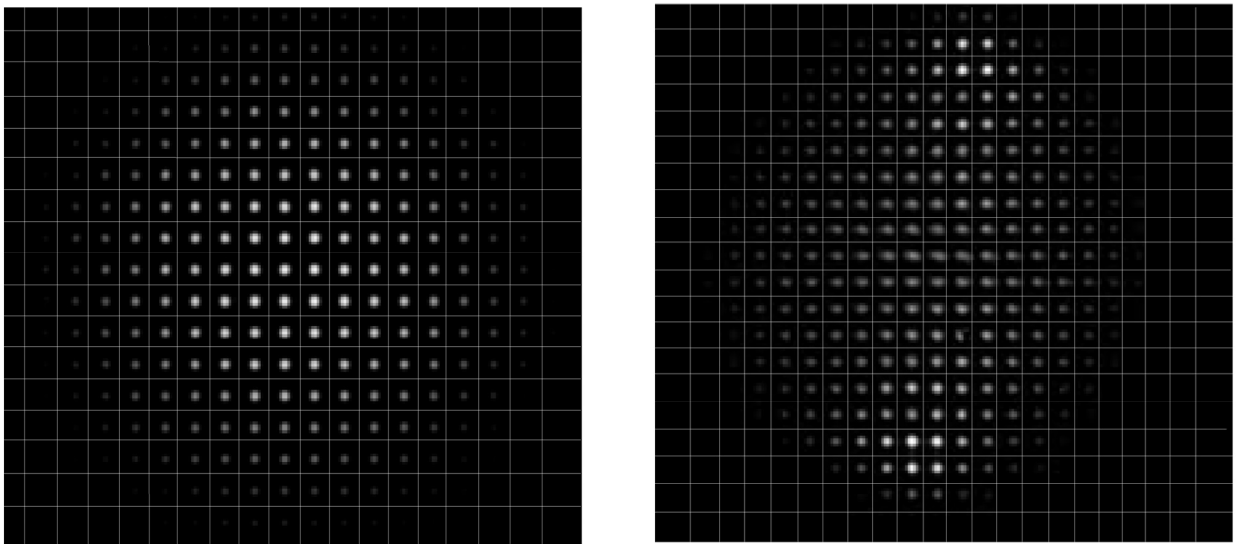

a) He-Ne laser **b) Diode laser**

The corresponding detector sub-aperture grids are indicated.

Figure 2 — Spot distributions obtained with Shack-Hartmann detector from He-Ne laser (left) and diode laser (right)

In the case of strong wavefront aberrations, the spots may spread out of their respective sub-apertures, leading to an erroneous wavefront evaluation. Measures shall be taken to avoid this effect, for example by a dynamic scaling of the sub-aperture grid.

The spot distribution $E(x, y)$ [$H(x, y)$ for pulsed laser beams] shall be recorded and stored in the electronic analysis system. Examples of measured distributions are shown in Figure 2.

6.4 Calibration

The calibration of the utilized Hartmann or Shack-Hartmann wavefront sensor shall be carried out as follows:

The sub-aperture screen to detector spacing L_H shall be determined either by mechanical measurement, or by comparison of the wavefront sensor results to known wavefronts. The calibration method shall be noted in the test report.

A known wavefront shall be recorded, providing a reference and may be either a spherical wave or a plane wave. Report the character and method for providing this reference wavefront in the test report.

The reference spot distribution $E_r(x, y)$ [$H_r(x, y)$ for pulsed laser beams] shall be acquired in the same way as described in 6.2 and stored in the electronic evaluation system (see Figure 3).

For a Shack-Hartmann sensor, it is important to employ a reference beam of identical wavelength, since aberrations in the lenslet array may lead to dispersion-induced displacements of the focal spots. Care shall be taken to avoid such effects.

Reference and signal beam may also be superposed and recorded simultaneously, permitting the correction of dynamical misalignment. It is necessary that provision be taken so that the detector electronics can discriminate between signal and reference by modulating the reference beam.

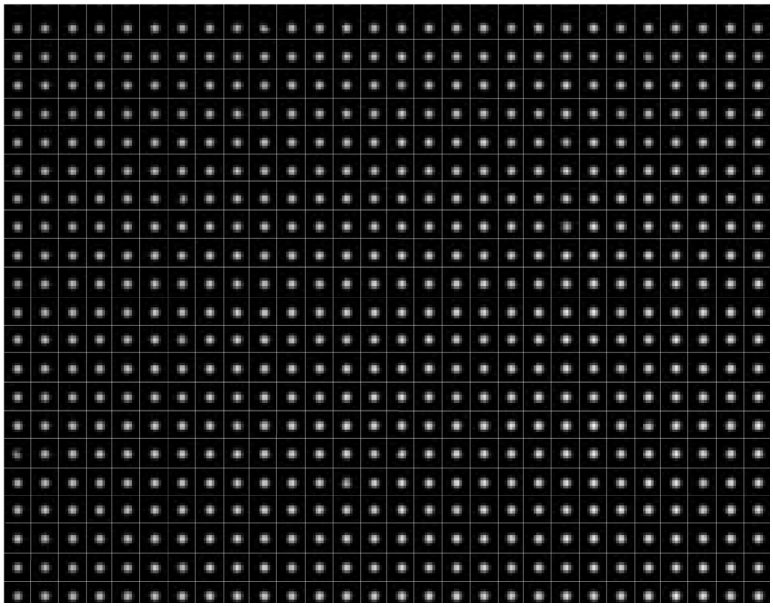

Figure 3 — Reference spot distribution (from collimated He-Ne laser) obtained with Shack-Hartmann detector and corresponding sub-aperture grid

The type and wavelength of the collimated beam used for calibration shall be recorded in the test report.

7 Evaluation of wavefront gradients

7.1 Background subtraction

Before wavefront evaluation, the acquired spot distribution $E(x, y)$ [$H(x, y)$] shall be properly corrected for background and noise effects. The provisions of ISO 13694 apply, providing either a background map or average background subtraction, or the clipping of the acquired distribution at a certain threshold power (energy) density $E_{\eta T}$ ($H_{\eta T}$).

For standard applications, distribution clipping provides an appropriate background correction. The value η chosen is such that $E_{\eta T}$ or $H_{\eta T}$ is just greater than the positive detector noise peaks. If the spot profile produced by the segmenting array exhibits structures in the outer wings (as often observed in case of diffractive lens elements), it is necessary to use larger offsets in order to compensate crosstalk with adjacent sub-apertures.

The utilized background correction technique and the chosen offset value $E_{\eta T}$ ($H_{\eta T}$) shall be specified in the test report.

7.2 Evaluation

The evaluation of the wavefront from the background corrected spot distribution $E'(x, y)$, the coordinates of each beamlet centroid, i.e. the first moment of an individual spot, shall be determined within the respective sub-aperture (ij) according to

$$x_{\mathrm{c},ij} = \frac{\iint\limits_{\mathrm{subap},ij} xE'(x,y)\mathrm{d}x\mathrm{d}y}{\iint\limits_{\mathrm{subap},ij} E'(x,y)\mathrm{d}x\mathrm{d}y} \text{ and } y_{\mathrm{c},ij} = \frac{\iint\limits_{\mathrm{subap},ij} yE'(x,y)\mathrm{d}x\mathrm{d}y}{\iint\limits_{\mathrm{subap},ij} E'(x,y)\mathrm{d}x\mathrm{d}y} \tag{12}$$

The computed spot positions $(x_\mathrm{c}, y_\mathrm{c})_{ij}$ shall be stored in memory.

In the same way, the spot distribution $E_\mathrm{r}(x, y)$ [$(H_\mathrm{r}(x, y)$] obtained from the reference beam shall be evaluated, yielding the reference positions $(x_\mathrm{r}, y_\mathrm{r})_{ij}$ for each sub-aperture, which shall be recorded in memory for comparison with the spot positions of the laser beam under test.

The local wavefront gradients $(\beta_x, \beta_y)_{ij}$ shall be evaluated from the coordinates of the beamlet centroids $(x_\mathrm{c}, y_\mathrm{c})_{ij}$ of the beam under test with respect to their reference positions $(x_\mathrm{r}, y_\mathrm{r})_{ij}$ according to

$$\begin{pmatrix} \partial w/\partial x \\ \partial w/\partial y \end{pmatrix}_{ij} = (\beta_x, \beta_y)_{ij} \approx \frac{1}{L_\mathrm{H}} \begin{pmatrix} x_\mathrm{c} - x_\mathrm{r} \\ y_\mathrm{c} - y_\mathrm{r} \end{pmatrix}_{ij} \tag{13}$$

NOTE For high-precision wavefront determination, a correction of the determined centroid positions with respect to a systematic trend of the power (energy) density over the area of each sub-aperture may be necessary (see Clause 9). The same statement applies (for Shack-Hartmann sensors) if the distance L_H is not set to exactly the focal length f of the lenslet array.

8 Wavefront reconstruction

8.1 General

From the measured gradient data [Equation (13)] the wavefront $w(x, y)$ can be reconstructed by various numerical methods. The most common techniques are direct numerical integration, matrix iterative and modal fitting techniques.

The method employed for wavefront reconstruction including the appropriate parameters and the degree of fit shall be identified in the test report.

8.2 Direct numerical integration (zonal method)

Using a suitable difference scheme, the wavefront gradients $(\beta_x, \beta_y)_{ij}$ at position (i, j) shall be approximated. The most appropriate difference scheme depends on the particular application and shall be recorded in the test report. Some approaches are suggested in A.1.

If the set of wavefront slopes appears to be inconsistent with a continuous wavefront ($\partial\beta_y/\partial x \neq \partial\beta_x/\partial y$), then a representation by a single surface is possible only in the least square sense.

The least square approach leads to the normal equations:

$$\boldsymbol{B}^{\mathsf{T}}\boldsymbol{C}^{-1}\boldsymbol{B}\cdot\vec{w} - \boldsymbol{B}^{\mathsf{T}}\boldsymbol{C}^{-1}\cdot\vec{\beta} = 0 \tag{14}$$

where

$\vec{w}$ is the wavefront vector as follows:

$$\vec{w} = \left(w^1, \ldots, w^{N\times M}\right)^{\mathsf{T}}$$

$\vec{\beta}$ is the $2N \times M$ wavefront gradient vector as follows:

$$\vec{\beta} = \left(\beta_x^1, \ldots, \beta_x^{N\times M}, \beta_y^1, \ldots, \beta_y^{N\times M}\right)^{\mathsf{T}}$$

$\boldsymbol{B}$ is the geometry matrix (A.2);

$\boldsymbol{C}$ is the noise covariance matrix.

For uncorrelated noise $\boldsymbol{C}$ becomes diagonal, representing the statistical measurement error of $\vec{\beta}$. The latter is estimated from the inverse square root of the power/energy density distribution.

The gradient information determines $w(x, y)$ only except for a constant, thus $\boldsymbol{B}^{\mathsf{T}}\boldsymbol{C}^{-1}\boldsymbol{B}$ becomes singular and standard linear equation solvers cannot be applied directly. The recommended strategy for solving Equation (14) uses the singular value decomposition (SVD) of $\boldsymbol{B}$. Matrix $\boldsymbol{B}$ depends only on the array geometry and the employed difference scheme, thus for stationary conditions the singular value decomposition has to be carried out only once, and subsequent wavefront reconstructions can be performed rather efficiently.

Alternatively, a matrix iterative approach may be used to solve for the wavefront vector directly. This eliminates the need for singular value decomposition and facilitates weighting the measurements by the appropriate irradiance values.

8.3 Modal wavefront reconstruction

The modal representation describes a wavefront by a polynomial expansion, as follows:

$$w(x, y) = \sum_{k=1}^{K} a_k \times P_k(x, y) \tag{15}$$

where

a_k are the coefficients;

P_k are the polynomial basis functions.

The most common basis sets are the Zernike polynomials (see Annex B) for circular and the Legendre, Hermite or Tchebyshev polynomials for rectangular sensor design, respectively. For special geometries, different sets are useful. The member functions shall be linearly independent but not inevitably orthogonal. The applied basis set shall be identified in the test report.

The local wavefront gradients are approximated by

$$\left.\frac{\partial w(x, y)}{\partial x}\right|_{ij} = \sum_{k=0}^{K} a_k \times \left.\frac{\partial P_k(x, y)}{\partial x}\right|_{ij} \quad \text{and} \quad \left.\frac{\partial w(x, y)}{\partial y}\right|_{ij} = \sum_{k=1}^{K} a_k \times \left.\frac{\partial P_k(x, y)}{\partial y}\right|_{ij} \tag{16}$$

The coefficients shall be determined by a least square approach, leading to a set of normal equations:

$$\boldsymbol{B}^{\mathsf{T}} \boldsymbol{C}^{-1} \boldsymbol{B} \cdot \vec{a} - \boldsymbol{B}^{\mathsf{T}} \boldsymbol{C}^{-1} \cdot \vec{\beta} = 0 \tag{17}$$

with $a = (a_1, ..., a_k)^{\mathsf{T}}$ and $\boldsymbol{B}$ given in A.2.

In solving Equation (17), a problem can arise if undersampling occurs, i.e. the number of modes projected out of the data exceeds the number of data points. Then higher order modes may perturb the solution and cause wavefront aliasing. In these cases, more data points shall be sampled or the number and form of the polynomials shall be examined very carefully.

9 Wavefront representation

The average tilt and tip shall be subtracted from the reconstructed wavefront $w(x, y)$ yielding the corrected wavefront $w_{\mathrm{c}}(x, y)$ (see ISO 15367-1:2003, 3.4.2). The corrected wavefront or the related phase distribution $\Phi_{\mathrm{c}}(x, y)$ shall be represented in the test report either as data table, vector diagram, three-dimensional distribution, contour plot or interferogram (see Figure 4).

If the focusabilty of the laser beam under test is important, the approximate spherical surface $s(x, y)$ (see ISO 15367-1:2003, 3.4.3) shall be subtracted from $w(x, y)$, in order to visualize the wavefront aberration function $w_{\mathrm{AF}}(x, y)$ (see Figure 5).

10 Uncertainty

10.1 General

General remarks on sources, estimation requirements and documentation of uncertainty connected with wavefront measurement are contained in ISO 15367-1. In 10.2 to 10.5, only those sources of uncertainty are considered which are relevant to Shack-Hartmann sensors.

10.2 Statistical measurement errors

Statistical measurement errors comprise mainly short-term source fluctuations and detector noise. The wavefront variance shall be calculated by standard error propagation from the power (energy) density distributions used for wavefront evaluation. Statistical fluctuations may be reduced by increasing the sampling period or by averaging over a number of measurements, provided the laser emission can be regarded as stationary.

There are two main contributions to statistical uncertainty:

a) noise or purely stochastic effects which may average to zero for a given sub-aperture,

b) bias or systematic effects which cause a given sub-aperture to give an incorrect reading.

The former [a)] is related to the precision of the measurement, while the later [b)] is related to the accuracy. These two contributions can be quite different for Shack-Hartmann (Hartmann) sensors, due to the limited number of detector elements employed for measuring the spot positions.

The wavefront measurement repeatability $w_{\mathrm{r,rms}}$ shall be determined according to 3.6 as the average of the r.m.s. difference between a single measurement and the average of the same wavefront. The time interval Δt between these measurements shall be chosen in a way to ensure that long-term drifts of sensor, source and environment can be neglected. The number of samples to be taken shall be at least 10.

Use a spherical or plane wavefront for measuring the wavefront repeatability.

The wavefront measurement accuracy $w_{\mathrm{a,rms}}$ shall be determined as specified in 3.7 as the average of the r.m.s. difference between a reference wavefront w_{r} and the tilt-corrected wavefront $w_{\mathrm{tc},n}$ after a certain amount of tilt θ_n has been applied to the reference wavefront. The time interval Δt between these measurements shall be chosen in a way to ensure that long-term drifts of sensor, source and environment can be neglected. The number of samples to be taken shall be at least 10 in two orthogonal directions, aligned to the detector reference system, and the tilt shall be varied between $-\beta_{\mathrm{max}}$ to β_{max} as defined in 3.5.

The recommended setup for the measurement of $w_{\mathrm{a,rms}}$ consists of a spherical wavefront emitted from a monomode fibre tip which is placed on an $x - y$ translation stage in the front focal plane of a highly corrected lens. A tilt θ_x of the plane wave obtained behind the lens is then related to the amount of translation x of the fibre and the focal length of the lens f by $\theta_x = x/f$.

10.3 Environmental effects

Variations in the measured parameters could be caused by temperature variation or mechanical vibration as well as by stray or ambient light. Temperature changes cause slow systematic deviations, e.g. drifts, and should be monitored with a supplementary sensor and, if possible, corrected in the final result. Thermal drifts shall be minimized by using appropriate warm-up times of beam source and sensor. Ambient and stray light give rise to a background signal which causes systematic errors in the centroid estimation of the Shack-Hartmann sensor. The background shall be carefully examined and subtracted from the measured signal.

10.4 Deficiencies in data acquisition

The signal-to-noise ratio and the uncertainty in the measurements is directly related to the spatial resolution of the Shack-Hartmann sensor, the finite sub-aperture diameter, the quantization process and non-linearities in signal amplification. Electronic timing jitter associated with CCD sensors will contribute to the cumulative error since it can cause uncertainty in pixel position. This is avoided by synchronizing CCD pixel clock and frame grabber or, alternatively, by a digital CCD camera.

NOTE 1 The quantization error gives only small contributions to the cumulative error even for an 8-bit ADC if the full dynamical range is available. In the presence of considerable background or undesirable beam-tail cut off, utilizing a 10-bit or even 12-bit ADC may be necessary.

NOTE 2 Hartmann wavefront sensors can cause an uncertainty in the wavefront gradient determination due to a variation of the power density over the area of a single pinhole of the segmenting array. This effect is small in most typical applications. For example, if the power density changes by 1 % over a pinhole diameter of 100 µm at a detector distance L_{H} = 10 mm, the wavefront gradient error is estimated to be of the order of 10 µrad only.

NOTE 3 The limited number of detector elements covered by the spot is often the dominant source of uncertainty.

10.5 Uncertainties due to geometrical misalignment

The contributions of misalignment effects to the cumulative uncertainty of particular importance for Shack-Hartmann sensors are mechanical shock, thermal instabilities or material degradation. An erroneous evaluation of centroid positions will result if the Shack-Hartmann detector is not properly positioned in the focal plane of the lenslet array. An axial displacement introduces an additional amount of positive or negative defocus. A lateral displacement of detector or array only generates an artificial tilt of the whole beam. Both contributions have no influence on the wavefront aberration function.

Severe systematic errors may occur for any additional rotation between detector and array. The resulting wavefront error is non-integrable and depends on the numerical wavefront reconstruction algorithm as well as on the amount of rotation. If there is any suspicion that mechanical misalignment has occurred, a re-calibration shall be performed immediately.

Deviation of the reference beam from the desired wavefront directly contributes to the measurement uncertainty in an additive way.

11 Test report

The test report shall at least contain the following information:

a) general information:

   1) reference to this part of ISO 15367 (ISO 15367-2:2005);

   2) date of test;

   3) name and address of test organization;

   4) name of individual performing the test.

b) information concerning the tested laser:

   1) laser type;

   2) manufacturer;

   3) manufacturer's model designation;

   4) serial number;

c) test conditions:

   1) laser wavelength(s) at which tested;

   2) temperature, expressed in kelvins (diode laser cooling fluid) (only applicable for diode lasers);

   3) operating mode [continuous wave (cw) or pulsed];

   4) laser parameter settings:

      i) output power or energy,

      ii) input current or energy,

      iii) pulse energy,

iv) pulse duration,

v) pulse repetition rate;

5) mode structure;

6) polarization;

7) environmental conditions;

d) information concerning testing and evaluation:

1) test method used:

i) Hartmann,

ii) Shack-Hartmann;

2) detector and sampling system:

i) manufacturer,

ii) model identifier,

iii) size of pinhole/lenslet array,

iv) array geometry,

v) distance array – detector L_H;

vi) Hartmann type:

— hole spacing d_x, d_y,

— hole diameter d_p;

vii) Shack-Hartmann type:

— lens spacing d_x, d_y,

— focal length f;

3) type of position sensitive detector:

i) pixel spacing,

ii) pixel size,

iii) dynamic range,

iv) response time,

v) trigger delay of sampling (for pulsed lasers),

vi) measuring time interval (for pulsed lasers);

4) location of measurement plane z_m;

5) beam forming optics and attenuating method:

i) type of attenuator,

ii) type of beam splitter,

iii) type of focusing element;

6) other optical components and devices used for the test (polarizer, monochromator, etc);

7) calibration of Shack-Hartmann detector:

i) type and wavelength of collimated reference beam,

ii) estimate of r.m.s. wavefront deformation of reference beam,

iii) date of calibration;

8) subtraction background:

i) type of subtraction technique,

ii) chosen offset value $E_{\eta T}$ ($H_{\eta T}$);

9) numerical method employed for wavefront reconstruction (zonal, modal):

i) zonal method: difference scheme used for numerical integration of $w(x, y)$,

ii) modal method:

— basis set (e.g. Zernike, Legendre, Hermite or Tchebyshev polynomials),

— degree of fit;

e) test results:

1) raw data: representation of measured wavefront gradients $(\beta_x, \beta_y)_{ij}$ by vector diagram (optional, see Figure 4 a);

2) wavefront: the evaluated corrected wavefront $w_C(x, y)$ and/or the wavefront aberration function $w_{AF}(x, y)$ shall be visualized by one of the following ways:

i) data table,

ii) three-dimensional distribution (see example in Figures 4 and 5),

iii) contour plot,

iv) interferogram;

3) evaluated wavefront related quantities:

i) defocus or radius of best sphere R_{SS},

ii) wavefront irregularity w_{PV},

iii) weighted r.m.s. deformation w_{rms},

iv) polynomial coefficients (modal wavefront reconstruction);

4) wavefront statistical uncertainty $w_{s,rms}$.

Dimensions in millimetres

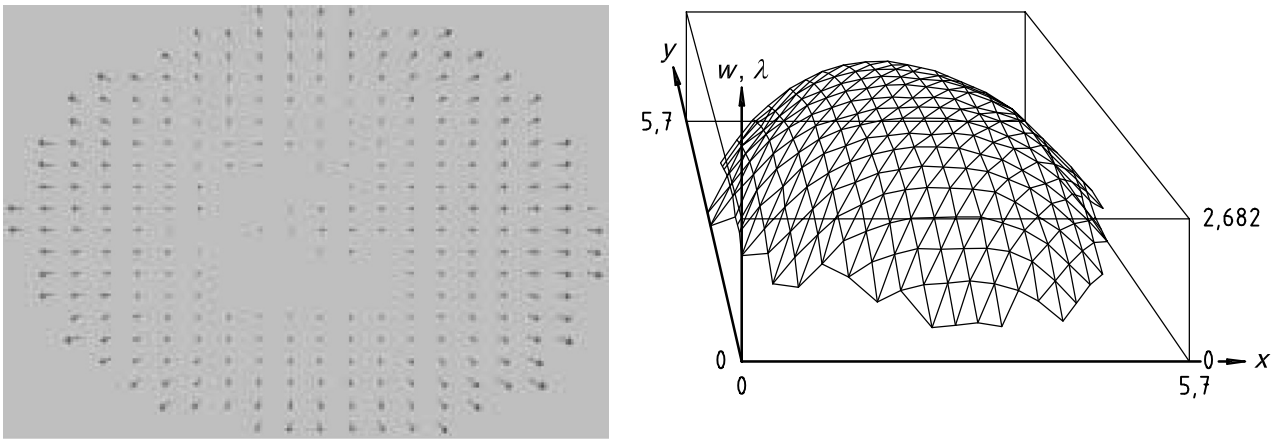

a) Measured wavefront gradients **b) 3D representation**

Figure 4 — Example for a vector diagram of the measured wavefront gradients and 3D representation of the reconstructed and corrected wavefront $w_c(x, y)$ of a diode laser (650 nm) obtained from Shack-Hartmann measurement

Dimensions in millimetres

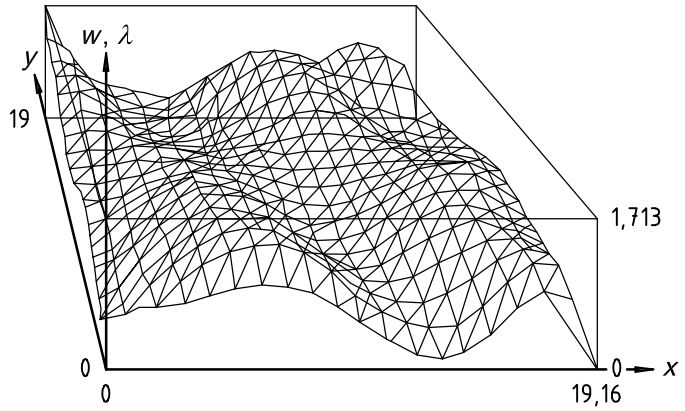

On the vertical axis the peak-to-valley wavefront irregularity w_{PV} is indicated.

Figure 5 — Example for a 3D representation of the wavefront aberration function $w_{AF}(x, y)$ of a femtosecond excimer laser (248 nm) obtained from a Hartmann measurement

Annex A
(informative)

Wavefront reconstruction

A.1 Difference schemes

From the measured gradient data $\beta_{x,y}^{ij}$, the wavefront can be reconstructed on a discrete point grid by numerical integration. To simplify the notation, a partition of the detector area into $N \times M$ rectangular sub-apertures indexed by (ij) is considered. However, if not stated otherwise, the expressions given below apply to more complicated detector geometries as well.

The first step is the employment of an appropriate difference scheme in order to get an approximation of $\beta_{x,y}^{ij}$:

$$\beta_x^{ij} = \frac{\partial w}{\partial x}_{ij} \approx \frac{1}{d_x} \sum_{k=-n}^{k=m} a_{i\times M+j}^{i\times M+j+k} w^{kj} \quad \text{and} \quad \beta_y^{ij} = \frac{\partial w}{\partial y}_{ij} \approx \frac{1}{d_y} \sum_{k=-n}^{k=m} b_{i\times M+j}^{i\times M+j+k} w^{ik} \tag{A.1}$$

Here, the order $n + m$ of the approximation as well as the Shack-Hartmann sub-aperture period d_x, d_y and the points w^{kj} and w^{ik} actually involved may vary from point to point. Moreover, it is possible to define β and w on different sub-grids. Some useful difference formulas for rectangular detector geometries are given in Table A.1.

Table A.1 — Selected difference schemes to be used for wavefront reconstruction

Gradient	Approximation	Error
$w'(x_0) = \beta_0 \approx$	$\frac{1}{2d_x}\left[w(x_0 + d_x) - w(x_0 - d_x)\right] \equiv \frac{1}{2d_x}(w_1 - w_{-1})$	$-\frac{1}{6} d_x^2 w'''(x_0)$
$w'(x_0) = \beta_0^x \approx$	$\frac{1}{12d_x}(w_2 - 8w_1 + 8w_{-1} - w_{-2})$	$\frac{1}{30} d_x^4 w^{(5)}(x_0)$
$w'(x_0) = \beta_0^x \approx$	$\frac{1}{60d_x}(w_3 - 9w_2 + 45w_1 - 45w_{-1} + 9w_{-2} - w_{-3})$	$\frac{1}{72} d_x^6 w^{(7)}(x_0)$
$w'(x_0) = \beta_0^x \approx$	$\frac{1}{2d_x}(-w_2 + 4w_1 - 3w_0)$	$\frac{1}{3} d_x^2 w'''(x_0)$
$w'(x_0) = \beta_0^x \approx$	$\frac{1}{d_x}(w_1 - w_0)$	$-\frac{1}{2} d_x w''(x_0)$
$w'(x_0) = \beta_0^x \approx$	$\frac{1}{12d_x}(-3w_4 + 16w_3 - 36w_2 + 48w_1 - 25w_0)$	$-\frac{1}{60} d_x^4 w^{(5)}(x_0)$

The non-symmetric schemes remain valid under change of sign (including subscripts). Non-rectangular detector geometries require the employment of adapted difference schemes. The applied scheme shall be identified in the test report.

A.2 Normal equations

As the wavefront gradient measurement is subject to noise and other sources of uncertainty, the wavefront reconstruction can be performed only in a least square sense, leading to:

$$\chi^2 = \frac{1}{\beta^2_{\text{rms},ij}} \sum_{i,j=0}^{N,M} \left[\left(\beta_{ij}^x - \frac{\sum\limits_{k=-n}^{k=m} a_{i \times M+j}^{i \times M+j+k} w^{kj}}{d_x} \right)^2 + \left(\beta_{ij}^y - \frac{\sum\limits_{k=-n}^{k=m} b_{i \times M+j}^{i \times M+j+k} w^{ik}}{d_y} \right)^2 \right] = \min \qquad \text{(A.2)}$$

for the direct reconstruction (see 8.1). The necessary condition for the solution of Equation (A.2) is

$$\vec{\nabla}_w \left(\chi^2 \right) = 0 \qquad \text{(A.3)}$$

which in turn leads to the normal equations:

$$\boldsymbol{B}^{\mathsf{T}} \boldsymbol{B} \cdot \vec{w} - \boldsymbol{B}^{\mathsf{T}} \vec{\beta} = 0 \qquad \text{(A.4)}$$

with the $2NM \times NM$ system matrix $\boldsymbol{B}$:

$$\boldsymbol{B} = \begin{array}{r} \text{row } 1 \\ \\ \\ \text{row } i \\ \\ \\ \text{row } N \times M \\ \\ \\ \\ \\ \\ \\ \text{row } 2N \times M \end{array} \left(\begin{array}{cccccccc} a_1^1 & a_1^2 & \ldots & & & & & a_1^{NM} \\ a_2^1 & \ldots & & & & & & \\ \ldots & & \ldots & & & & & \\ \ldots & a_i^{i-n} & \ldots & a_i^{ii} & \ldots & a_i^{i+m} & & \\ & & & & \ldots & & & \\ & & & & & \ldots & & \\ & & & & & & & a_{NM}^{NM} \\ b_1^1 & \ldots & & & & & & b_1^{NM} \\ \ldots & . & & & & & & \\ \ldots & & & & & & & \\ \ldots & b_i^{i-n} & \ldots & b_i^{i-n} & \ldots & b_i^{i+m} & & \\ & & & & \ldots & & & \\ & & & & & \ldots & & \\ & & & & & & & b_{NM}^{NM} \end{array} \right) \qquad \text{(A.5)}$$

$$\begin{array}{cc} \text{column } 1 & \text{column } N \times M \end{array}$$

If, however, the wavefront statistics are known, the best linear unbiased estimate of w shall be calculated according to

$$\boldsymbol{B}^{\mathsf{T}} \boldsymbol{C}^{-1} \boldsymbol{B} \cdot \vec{w} - \boldsymbol{B}^{\mathsf{T}} \boldsymbol{C}^{-1} \vec{\beta} = 0 \qquad \text{(A.6)}$$

with the $2NM \times 2NM$ wavefront covariance matrix $\boldsymbol{C}$. In the case of any additional detector or ambient noise with covariance matrix $\boldsymbol{C}_n$, a Wiener estimate may lead to an even smaller mean square error:

$$\left[\boldsymbol{B}^{\mathsf{T}} \boldsymbol{C}^{-1} \boldsymbol{B} + \boldsymbol{C}_n^{-1} \right] \cdot \vec{w} - \boldsymbol{B}^{\mathsf{T}} \boldsymbol{C}^{-1} \vec{\beta} = 0 \qquad \text{(A.7)}$$

Annex B
(informative)

Zernike polynomials for representation of wavefronts

The Zernike polynomials $Z_{nl}(\rho,\varphi)$ form a complete orthonormal set for the interior of the unit circle in the real plane [1]. Therefore, they are of particular importance for problems with circular apertures and can be written in complex form:

$$Z_{nl}(\rho,\varphi) = R_{nl}(\rho) \times e^{\pm il\varphi} \tag{B.1}$$

with $n \geqslant l \geqslant 0$ and $n - l$ even. Equation (B.1) can be rewritten in real form by introducing even (e) and odd (o) functions $Z^{e,o}$ for each pair (n,l):

$$Z_{nl}^{e,o}(\rho,\varphi) = R_{nl}(\rho) \times \begin{cases} \cos(l\varphi) & \text{(even)} \\ \sin(l\varphi) & \text{(odd)} \end{cases} \tag{B.2}$$

The explicit expression for the radial polynomials R_{nl} is given by

$$R_{nl}(\rho) = \sqrt{2(n+1)} \sum_{m=0}^{(n-l)/2} \frac{(-1)^m (n-m)!}{m! \times \left[0{,}5(n+l)-m\right]! \times \left[0{,}5(n-l)-m\right]!} \rho^{n-2m} \tag{B.3}$$

Table B.1 gives explicit expressions for some of the first Zernike polynomials.

Table B.1 — First Zernike polynomials and corresponding type of aberration

Zernike polynomial		Expression	Type of aberration
$Z_{0,0}$	(Z_0)	1	Piston
$Z_{1,1}^{e}$	(Z_1)	$\rho\cos(\varphi)$	Tip
$Z_{1,1}^{o}$	(Z_2)	$\rho\sin(\varphi)$	Tilt
$Z_{2,0}$	(Z_3)	$2\rho^2-1$	Defocus
$Z_{2,2}^{e}$	(Z_4)	$\rho^2\cos(2\varphi)$	Astigmatism
$Z_{3,1}^{e}$	(Z_6)	$(3\rho^2-2)\,\rho\cos(\varphi)$	Coma
$Z_{4,0}$	(Z_8)	$6\rho^4-6\rho^2+1$	Spherical aberration
NOTE Nomenclature in brackets corresponds to ISO 10110-5.			

The Zernike representation of a wavefront $w(\rho,\varphi)$ therefore writes:

$$w(\rho,\varphi) = \sum_{n=0}^{\infty} \sum_{l=0}^{n} \left[a_{nl}^{e} \times \cos(l\varphi) + a_{nl}^{o} \times \sin(l\varphi) \right] \times R_{nl}(\rho) \tag{B.4}$$

Bibliography

[1] BORN, M. and WOLF, E. *Principles of Optics*, 7th ed., Cambridge Univ. Press, 1999, pp. 523-525 and pp. 905-910

[2] TYSON, R.K. *Principles of Adaptive Optics*, 2nd ed., Academic Press, 1998

[3] VETTERLING, W.T. TEUKOLSKY, S.A. PRESS, W.H. FLANNERY, B.P. *Numerical Recipes in C*, 2nd ed., Cambridge University Press, 1992

[4] ISO 9334, *Optics and optical instruments — Optical transfer function — Definitions and mathematical relationships*

[5] IEC 61040, *Power and energy measuring detectors, instruments and equipment for laser radiation*

[6] ISO 10110-5, *Optics and optical instruments — Preparation of drawings for optical elements and systems — Part 5: Surface form tolerances*

[7] ISO 11146-1, *Lasers and laser-related equipment — Test methods for laser beam widths, divergence angles and beam propagation ratios — Part 1: Stigmatic and simple astigmatic beams*

[8] ISO 11146-2, *Lasers and laser-related equipment — Test methods for laser beam widths, divergence angles and beam propagation ratios — Part 2: General astigmatic beams*

ICS 31.260

Price based on 20 pages